Originally published 9 April 2010; corrected 8 December 2010

www.sciencemag.org/cgi/content/full/328/5975/195/DC1

Supporting Online Material for

Australopithecus sediba: A New Species of *Homo*-like Australopith from South Africa

Lee R. Berger,* Darryl J. de Ruiter, Steven E. Churchill, Peter Schmid, Kristian J. Carlson, Paul H. G. M. Dirks, Job M. Kibii

*To whom correspondence should be addressed. E-mail: profleeberger@yahoo.com

Published 9 April 2010, *Science* **328**, 195 (2009)
DOI: 10.1126/science.1184944

This PDF file includes

Correction: In table S2, a typographical error led to computational errors in the brachial and relative humeral length indices. The brachial index was given as 87.9 but should have been 84.3. The range of relative humeral length indices was given as 7.86-8.15 but should have been 8.15-8.23.

TEXT S1. Fossil preservation, ontogenetic age, and sex of Malapa hominins

Recent discoveries at the site of Malapa include associated craniodental and postcranial remains of at least two individuals. The two skeletons were found in the same stratigraphic horizon, dated to between 1.95-1.78 Ma, and separated from one another by no more than half a meter horizontally. The remains of one individual (MH2) were recovered in partial articulation, while those of the other (MH1) were somewhat more disturbed, yet still in close association (distributed over an area of less than 2 m^2). The majority of the hominin fossils are in very good condition, and this, combined with the spatial distribution of the skeletons, the partial articulation of one individual (and of some of the associated faunal remains), and the geological context indicates rapid deposition and contemporaneity of the two hominin individuals (*1*).

MH1 is a partial skeleton preserving much of the cranium and a partial mandible, maxillary and mandibular teeth, and portions of the postcranial axial skeleton, pectoral girdle, upper limb, pelvic girdle, and lower limb (Table S1). The first element of MH1 found (UW 88-1, clavicle) was discovered by Matthew Berger on August 15, 2008. Secondary growth centers of the proximal humerus, humeral medial epicondyle, proximal ulna, distal radius, os coxa and proximal femur were unfused at the time of death, while that of the distal humeral epiphysis was fused. Mandibular and maxillary permanent canines, M1s and M2s and the right I^1 exhibit slight to moderate occlusal attrition. Radiographic examination and virtual preparation demonstrates that the maxillary and mandibular M3 crowns are nearing completion, but lacking root development. The state of postcranial epiphyseal fusion and the degree of development of the M3 crowns leads to the provisional conclusion that MH1 was at a developmental stage equivalent to a modern human child of 12 -13 years (*2*), making this specimen roughly comparable in physiological age to the type specimen of *H. habilis* (OH 7: (*3*)) and the *H. erectus* (*ergaster*) individual from Nariokotome (KNM-WT 15000: (*4*)). Pronouncement of the supraorbital torus and glabellar prominence, eversion of the gonial region of the mandible, pronouncement of the canine jugae, and relatively large and rugose muscle scars in the postcranial skeleton (despite the juvenile status of the individual) all support the suggestion that MH1 was a male. The sciatic notch of MH1 is fairly wide (stage 2 of Walker (*5*)), but this character state is plesiomorphic for the genus *Homo* (*6*) and also is commonly seen in modern human juvenile males (*5*). Thus, a fairly wide sciatic notch is not inconsistent with the diagnosis of a male individual.

MH2 is represented by an incomplete mandible, maxillary and mandibular teeth, and portions of the postcranial axial skeleton, pectoral girdle, upper limb, pelvic girdle, and lower limb (Table S1). The first element of MH2 (UW 88-57, humerus) was found by Lee Berger on September 4, 2008. Adult status for MH2 is indicated by full ossification, with obliterated fusions lines, of all observable epiphyseal plates, and by moderate-to-heavy wear of the maxillary and mandibular molars, including the M3s. The mandibular ramus is small in height relative to that of MH1, and the preserved but damaged gonial region evinces less eversion (the gonial region in MH2 is damaged, and owing to displacement of its inferior border it appears to exhibit slight-to-moderate eversion; however, we judge that reconstruction of the MH2 mandible would greatly reduce or even eliminate this apparent eversion). While the ramus of MH2 is slightly anteroposteriorly broader than that of MH1, the juvenile has not completed ramal growth. Despite this, the MH1 ramus at its present ontogenetic stage is already taller than the adult morphology exhibited by MH2, while both corpora are approximately equal in robusticity (Fig. S2). The pubic body of the os coxa is mediolaterally broad and square in shape, and the

postcranial muscle scars are generally weakly-to-moderately rugose, all suggesting that MH2 was a female.

TEXT S2. Comparative craniodental materials examined in this study.

Au. afarensis. The samples attributed to *Au. afarensis* from Hadar, Laetoli, and the Middle Awash were utilized. For this taxon we relied on published reports (*7*) and casts.
Au. africanus. The samples attributed to *Au. africanus* from Taung, Sterkfontein and Makapansgat were employed. Original specimens were examined first-hand.
Au. garhi. The cranium BOU-VP-12/130 from Bouri was included, with data taken from a published report (*8*).
Au. aethiopicus. The cranium KNM-WT 17000 was examined first-hand for this study.
Au. boisei. Samples from the Omo Shungura sequence, East Lake Turkana, and Olduvai Gorge were included in this study. Original specimens from East Lake Turkana were examined first-hand, while casts and published reports (*9*) were used to study the Omo and Olduvai materials.
Au. robustus. The samples from Kromdraai, Swartkrans, Sterkfontein, Drimolen, Gondolin, and Coopers were included in this study. First-hand observations of original specimens from all localities were used with the exception of Drimolen fossils, which were compared using published reports (*10, 11*).
H. habilis. Samples from Olduvai Gorge, East Lake Turkana, the Omo Shungura sequence, and Hadar were included in this study. Original East Lake Turkana fossils were examined first-hand, while for the Olduvai, Omo, and Hadar materials we relied on casts and published reports (*12, 13, 14*). We include the following fossils in the hypodigm of *H. habilis*: AL 666-1, KNM-ER 1478, KNM-ER 1501, KNM-ER 1502, KNM-ER 1805, KNM-ER 1813, KNM-ER 3735, OH 4, OH 6, OH 7, OH 13, OH 15, OH 16, OH 21, OH 24, OH 27, OH 31, OH 37, OH 39, OH 42, OH 44, OH 45, OH 62, and OMO-L894-1.
H. rudolfensis. Samples from Olduvai Gorge, East Lake Turkana, and Lake Malawi were included in this study. The East Lake Turkana fossils were examined first-hand, while for the Olduvai and Lake Malawi fossils we relied on casts and published reports (*15, 16*). We include the following fossils in the hypodigm of *H. rudolfensis*: KNM-ER 819, KNM-ER 1470, KNM-ER 1482, KNM-ER 1483, KNM-ER 1590, KNM-ER 1801, KNM-ER 1802, KNM-ER 3732, KNM-ER 3891, OH 65, and UR 501.
H. erectus. Samples from Baringo, Chemeron, Dmanisi, East and West Lake Turkana, Konso, Olduvai Gorge, Sangiran, Swartkrans, Tighenif, Trinil, and Zhoukoudian were included in this study. In particular, the following specimens from Swartkrans are considered to represent *Homo erectus*: SK 15, SK 18a, SK 27, SK 43, SK 45, SK 68, SK 847, SK 878, SK 2635, SKW 3114, SKX 257/258, SKX 267/2671, SKX 268, SKX 269, SKX 334, SKX 339, SKX 610, SKX 1756, SKX 2354, SKX 2355, SKX 2356, and SKX 21204. It has been suggested (*17, 18*) that SK 847 and Stw 53 might represent the same taxon, and that this taxon is a currently undiagnosed species of *Homo* in South Africa. However, we agree with Clarke (*19, 20*) that SK 847 can be attributed to *H. erectus*, and that Stw 53 represents *A. africanus*. Since there is no clear indication that more than one species of *Homo* is represented in the Swartkrans sample, we consider all this material to belong to *H. erectus*. Original Baringo, Chemeron, Lake Turkana and Swartkrans fossils were all examined first-hand, while the remainder were based on casts and published reports (*21, 22, 23, 24, 25*).

TEXT S3. Character states based on measures from Table 2

Here we describe the character states displayed in Table 1 that are based on measurements presented in Table 2.

1. Cranial capacity: <600=small; 600-700=intermediate; >700=large
5. Postorbital constriction index: >80=slight; 71-79=moderate; <70=marked
6. Horizontal distance between the TMJ and M^2/M^3: <58=short; >58=long. MH1 does not have the M^3 erupted, thus additional growth would almost certainly influence this measure; however, we judge that such growth would not exceed the 58mm cutoff length required to necessitate a designation of long.
7. Facial prognathism: <65=prognathic; 65-70=mesognathic; >70=orthognathic. For this measure we use the sellion-prosthion angle since the M^3 of MH1 is not yet erupted. We note that additional growth in MH1 might have altered this angle.
9. Anteromedial (A-M) incursion of temporal lines on frontal bone based on minimum frontal breadth (ft-ft): >60=weak; 40-60=moderate; <40=strong
25. Inferior nasal bridge breadth: <10=narrow; >10=wide
31. Malar thickness: <15=thin; >15=thick
32. Infraorbital foramen height relative to the inferior orbital margin: >20=low; <20=high
35. Masseter origin index: <100=low; >100=high
38. Subnasal projection index: <100=weak; 100-150=moderate; >150=marked
50. Mandibular corpus cross sectional area at M_1: <700=small; >700=large
57. Maxillary post-canine crown area: <700=small; 700-800=moderate; >800=large
59. Mandibular molar crown area: <500=small; 500-600=moderate; >600=large
60. Maxillary incisor to post-canine ratio: <12=small; 12-20=moderate; >20=large
61. Maxillary canine to post-canine ratio: <10=small; >10=large
62. Mandibular canine to post-canine ratio: <10=small; >10=large

TEXT S4. Digital reconstruction and virtual preparation

Virtual preparation of specimens was undertaken when mechanical preparation was no longer feasible (e.g., Figs. S1 and S5). The protocol for virtual preparation of a volume is briefly described. Through the use of computed tomography (CT), serial stacks of images representing entire fossils were acquired (e.g., 500 images for MH1 cranium). CT scanning was performed at Johannesburg Hospital (Johannesburg, South Africa) on a Philips Brilliance 16P medical CT scanner (Philips Healthcare, Andover, MA). Bone reconstruction algorithms were applied to raw scan data in order to produce image stacks (DICOM format) that could be used in subsequent analyses. Pixel dimensions in images ranged between 0.23 – 0.47 mm, depending on object size, while scan slice thickness was always 0.8 mm, and reconstruction increment always 0.4 mm (i.e., space between images). An attempt was made to use isotropic voxels (e.g., 0.4 mm), whenever specimen size made it feasible.

Following data acquisition, image stacks were segmented to produce isosurfaces using Avizo 6.1 software (Visualization Sciences Group, Mérignac, France). During the creation of an isosurface, threshold choices were verified using external dimensions of exposed morphology on specimens in order to corroborate equivalent dimensions of morphology on rendered specimens. Minor variations in threshold choice had very little effect on these dimensions. When possible, automated segmentation routines were used to render volumes. When automated routines were not feasible, for example when specimen and matrix densities were too similar, rendering was performed by manual segmentation. In the latter case, image stacks were assessed in three orthogonal directions, one of which was determined by the orientation of the original scan plane. The decision to include an individual voxel within a rendered volume was finalized after consulting each of the three orthogonal views, as well as voxels in the same line of sight through the preceding and following images of the stack. When more extensive preparation was required (e.g., the cranium of MH1, see Fig. S1), this process was repeated a second time.

In order to estimate cranial capacity on the rendered cranium of MH1, the left parietal and portions of the articulating left temporal squama were duplicated and mirror-imaged to fill-in missing morphology on the right side of the cranium. The mirror-imaged bones were aligned by including areas of overlap between existing frontal and temporal bones on the right side and mirror-imaged areas from the left side. In this way, curvatures could be aligned and the shape of the cranial vault estimated. We recognize that this approach reduces bilateral asymmetry in vault shape, but we note that the area of overlap was minimized to the extent possible and we balanced this criterion with the importance of aligning the mirror-imaged areas.

The cranial vault reconstruction is missing only the occipital, petrous portions of both temporal bones, and small areas of the parietal bones along the length of the sagittal suture. The endocranial surface of the reconstructed vault, including the duplicated and mirror-imaged portion on the right side of the cranial vault, was isolated and rendered. The volume of the rendered partial endocast is 363 cc. There are two regions that must be added to the partial endocast volume in order to complete it, both of which must be estimated: a small posteriorly-located area containing much of the occipital lobes, and specifically the occipital poles, and the posterior cranial fossa. The missing portion at the posterior aspect of the cranium is estimated to be approximately 7-10 cc. This estimate is based on comparable volumes that were removed or added to the endocast during early stages of its virtual reconstruction. Estimating size of the missing posterior cranial fossa is less straightforward. Two australopith (AL 23000 and STS 19) cerebellar volumes are reported as 40-50 cc, while three early members of the genus *Homo*

(KNM-ER 1813, KNM-ER 1805, and KNM-ER 1470) have cerebellar volumes approximately ranging between 55-75 cc (*26*). A conservative estimate of 50 cc for the posterior cranial fossa of the MH1 juvenile, therefore, seems justified. This is the basis for the minimum estimated cranial capacity of 420 cc (363 cc + 7 cc + 50 cc).

Humeral and femoral specimens of MH1 and MH2 were CT scanned and rendered using the same procedure as outlined above. In order to create diaphyseal cross sections, humeral and femoral medullary spaces were identified and matrix was subtracted following the same manual segmentation procedure as outlined above. Subsequently, humeral regions of interest (e.g., midshaft and mid-proximal diaphysis) were identified on virtual specimens, cross sections obtained, and cross-sectional geometric properties calculated following an established protocol (*27, 28, 29*). Femoral regions of interest (e.g., mid-proximal diaphyses) were identified on virtual specimens using a chimpanzee femur in order to estimate approximate location along the diaphysis of MH1. This was accomplished by overlapping the MH1 specimen onto the proximal region of a chimpanzee femur, then orientating the MH1 reconstructed proximal femur following established criteria (*27, 28, 29*). A chimpanzee femur was selected because of a greater assumed similarity with MH1 in overall length than comparative human femora. If absolute femur length of MH1 ultimately resembles modern human length more than chimpanzee length, then the percent length of the femoral cross section of interest would increase (e.g., 75% rather than 70%, etc.). Once positioned correctly, cross sections of the diaphysis were obtained, and cross-sectional geometric properties were calculated following the established protocol (*27, 28, 29*).

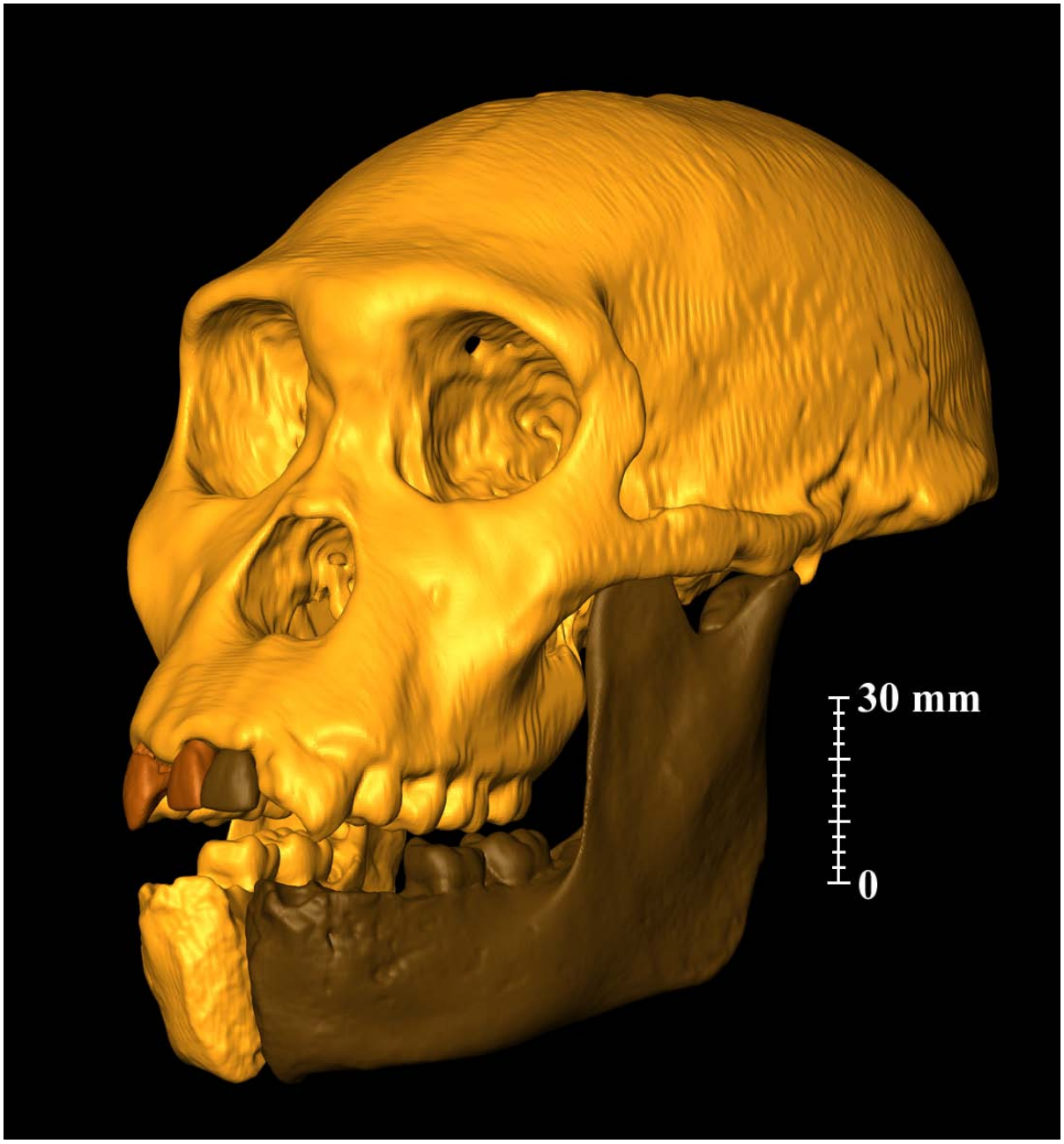

Figure S1. Virtual reconstruction of the skull of MH1. Orange signifies intact portions of the cranium and mandible that were manually segmented from the surrounding matrix. Copper-colored teeth signify isolated teeth that were virtually refit to the rendered cranium. Brown signifies mirror-imaged antimeres. See Text S4 for details of the virtual reconstruction process.

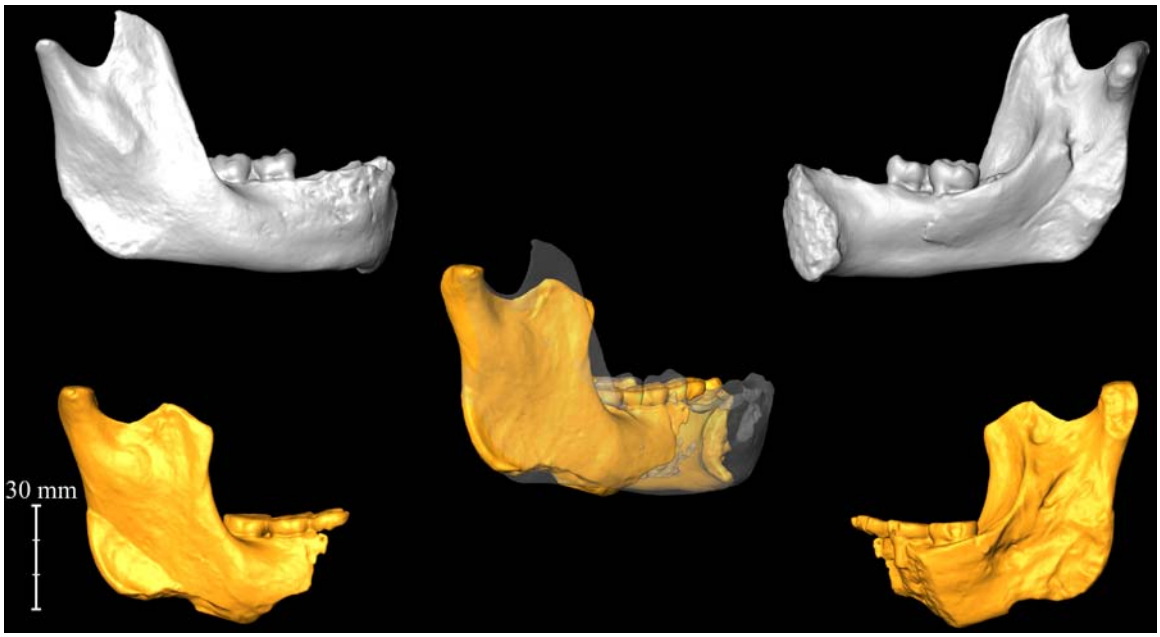

Figure S2. Virtual reconstructions of the mandible of MH1 (grey) in (a) lateral and (b) medial views, and MH2 (orange) in (c) lateral and (d) medial views. We overlap the specimens (e), aligning them at the condyle. Note that although the ramus of the adult female MH2 is anteroposteriorly broader, the ramus of the juvenile male MH1 (transparent) is already taller, indicating some degree of sexual dimorphism.

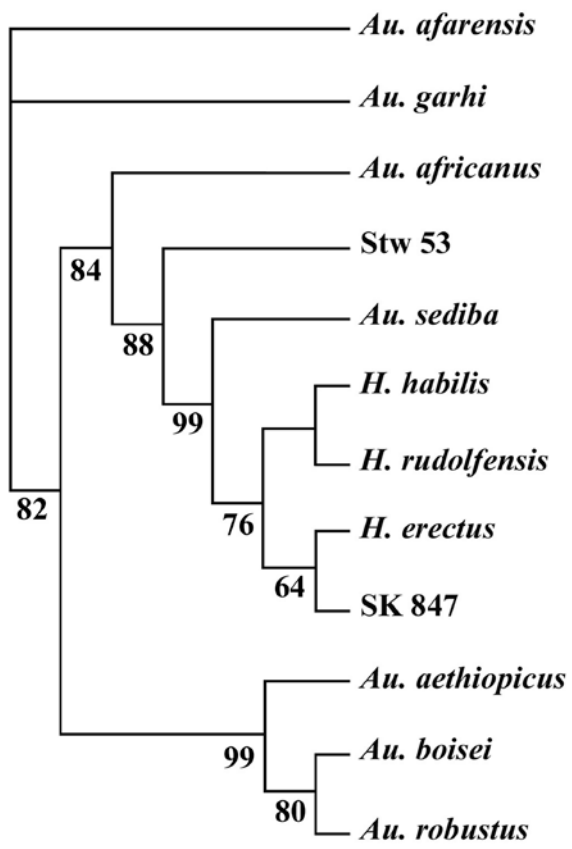

Figure S3. Most parsimonious cladogram produced from the characters presented in Table 1, using PAUP 4.0 (beta version 10). Tree length is 128 steps if character states are unordered and multistate characters are treated as either uncertainties or as variable; tree length is 137 steps if character states are ordered and multistate characters are treated as either uncertainties or as variable; tree length is 165 if character states are unordered and multistate characters are treated as polymorphisms, and 175 steps if character states are ordered and multistate characters are treated as polymorphisms. When run with unordered character states, only one tree results; when run with ordered character states, two trees result: the one presented here, and another where KNM-ER 1470 resides with the *H. erectus*/SK 847 clade. The consistency index is 0.672, the homoplasy index is 0.328, and the retention index is 0.744. Bootstrap numbers are based on 10000 replicates. The inclusion of postcranial character states in the phylogenetic analysis would necessitate the exclusion of *H. rudolfensis* from the analysis. Also, the postcranial features that *Au. sediba* shares with *Homo* are found primarily in the os coxa, an element that is completely unrepresented in *H. habilis*. Taxonomic diagnoses and phylogenetic interpretations are generally based on craniodental remains, which necessitate such a focus even in taxa such as *Au. sediba* that preserve a more complete representation of the skeleton. This is not to say, however, that postcranial attributes cannot enlighten phylogenetic studies, and for these reasons the significance of the postcranial morphology of Malapa is discussed. What is important is that the postcranial remains support phylogenetic inferences derived from study of the craniodental material.

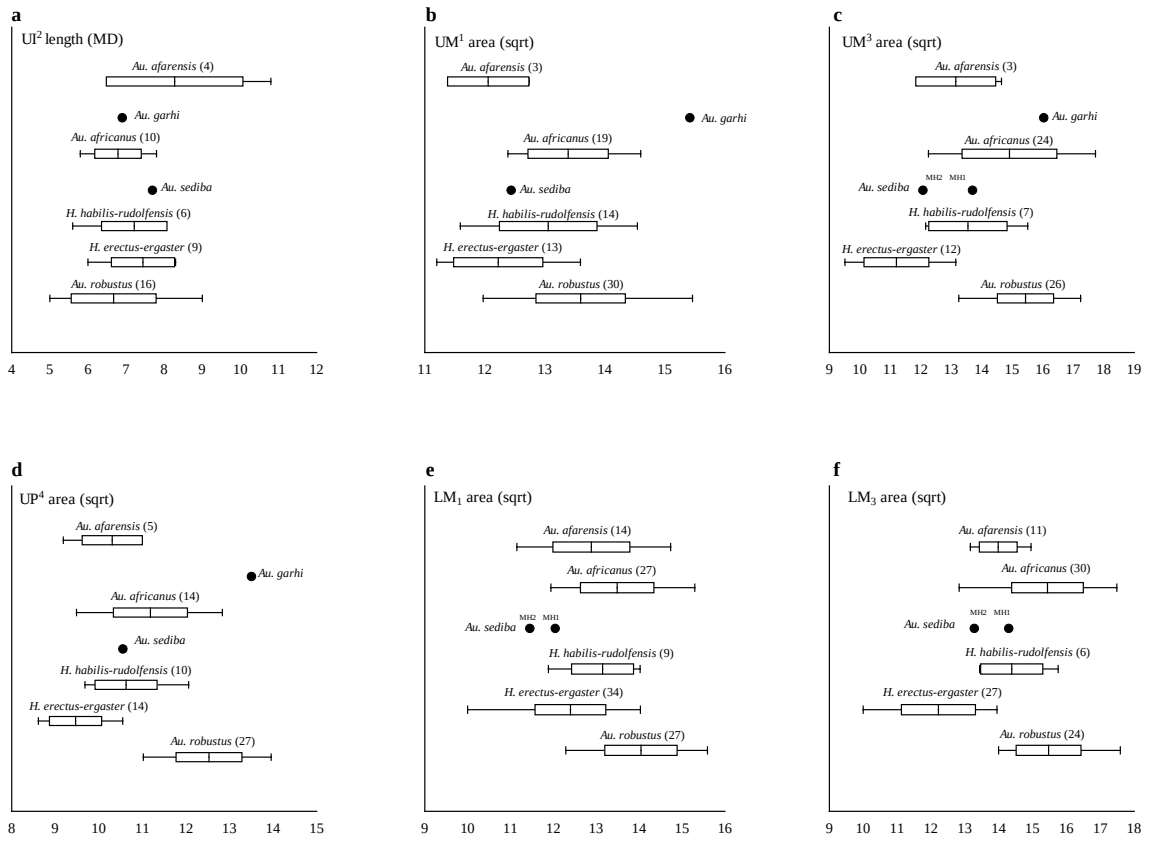

Figure S4. Dental size of *Au. sediba* compared to other early hominin taxa. These are additional teeth preserved in MH1 and MH2 that were not included in Fig. 3 in the main text. Owing to small sample sizes, *H. habilis* and *H. rudolfensis* samples were combined. (a) Upper lateral incisor MD length; (b) Square root of calculated (MD x BL) upper first molar area; (c) Square root of calculated (MD x BL) upper third molar area; (d) Square root of calculated (MD x BL) upper fourth premolar area; (e) Square root of calculated (MD x BL) lower first molar area; (f) Square root of calculated (MD X BL) lower third molar area. Measures taken on original specimens by DJD for *Au. africanus*, *Au. robustus*, and *Au. sediba*. Measurements for *Au. afarensis*, *H. habilis*, *H. rudolfensis*, and *H. erectus* from (*30*).

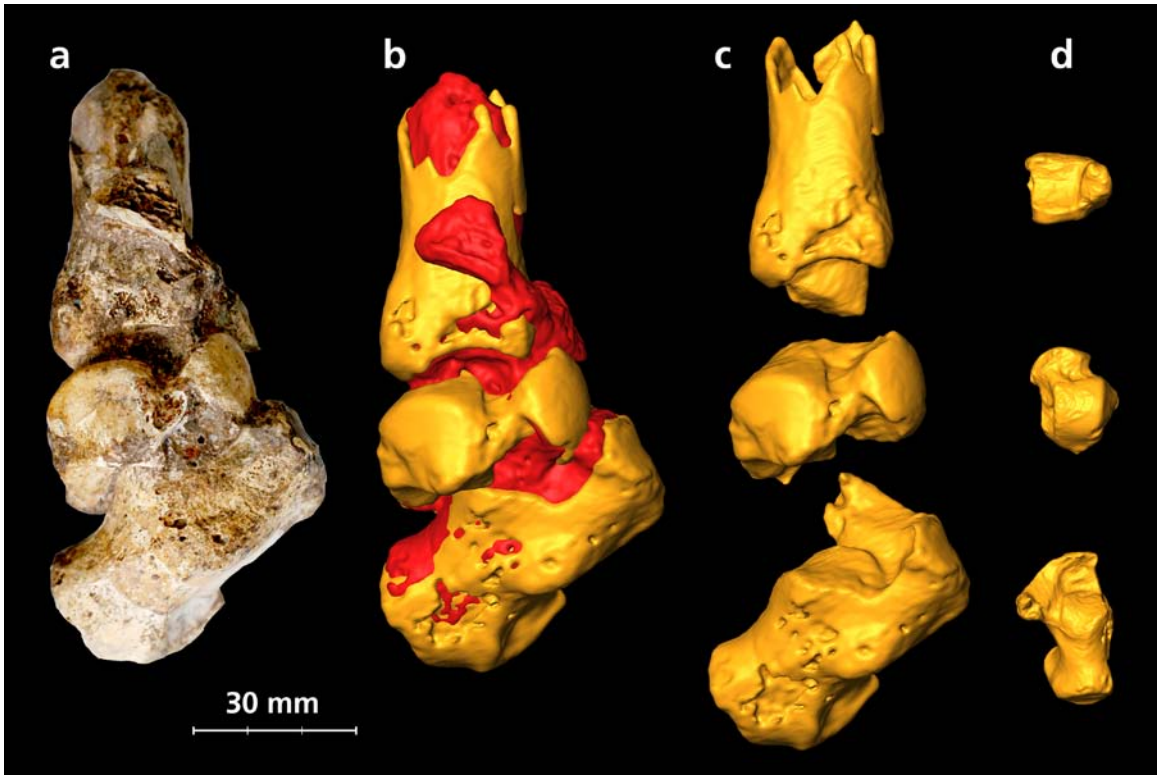

Figure S5. Right distal tibia, talus and calcaneus of MH2, illustrating the virtual separation of elements undertaken to allow for measurement of the talus as reported in SOM Table S2: (a) partial leg and foot skeleton as preserved, showing tibia, talus and calcaneus in near-anatomical relationship and cemented together with calcified sediment; (b) virtual reconstruction of the partial leg and foot skeleton, with areas of calcified sediments indicated in red; (c) distal tibia (top), talus (middle) and calcaneus (bottom) after virtual removal of calcified sediment and separation of the elements; (d) virtual reconstructions of tibia in inferior view (top) and talus (middle) and calcaneus (bottom) in superior view, all at 50% of size of elements depicted in the other three columns.

Table S1: List of elements currently attributed to MH1 and MH2[a]

Element	Catalog number
Malapa Hominin 1 (MH1)	**UW88[b]**
Cranium with RP^3-M^3, LI^2 and LP^3-M^3	50
Cranial vault fragments (2)	31, 32
Right I^1	29
Right C^1	30
Right hemi-mandible with erupted RM_1, RM_2 and unerupted RM_3 crown	8
LC_1 with anterolateral wall of mandibular corpus	2
Cervical vertebrae (3)	9, 72, 83
Thoracic vertebrae (3)	11, 37, 69
Thoracic vertebral fragments (2)	70, 90
Rib fragments (6)	13, 15, 17, 41, 74, 86
Lumbar vertebra (1)	92
Acromial end and lateral shaft of right clavicle	1
Scapular fragment (root of spine)	113
Right humerus (3 conjoined pieces: lacking proximal epiphysis)	34, 42, 88
Left proximal humeral metaphysis/diaphysis	36
Right proximal ulna	3
Distal epiphysis of right radius	12
Right third metacarpal	112
Inferior portion of right ilium (2 conjoined pieces)	6, 7
Left ilium and associated fragments	67, 68, 102
Left ischium	14
Right proximal femur (4 conjoined pieces)	4, 5, 39, 89
Right distal tibia (2 conjoined pieces)[c]	21, 40
Metatarsal diaphyses (2)	16, 22
Malapa Hominin 2 (MH2)	**UW88[b]**
Partial left M^2	19
Left M^3	20
Partial right mandible with M_1-M_3	54
Partial left mandibular corpus with M_3 and partial M_2	55
Cervical vertebra (1)	93
Thoracic vertebrae (3)	43, 44, 96
Right first rib	58
Right rib (complete)	61
Rib fragments (6)	45, 46, 47, 48, 59, 60
Acromial end and lateral shaft of right clavicle	38
Acromial end of left clavicle	94
Right scapula (2 conjoined pieces)	56
Left scapular glenoid fossa	104
Left scapular acromion process	103

Right humerus	57
Left humeral head	101
Right ulna	62
Right radius	85
Left capitate	105
Right hamate	95
Left hamate	106
Right metacarpals I, II, III, IV and V	115, 116, 117, 118, 119
Right manual proximal phalanges (2)	108, 120
Right manual intermediate phalanges (3)	121, 122, 123
Right manual distal phalanx	124
Right pubis	52
Left ischiopubic ramus and partial pubic symphysis	10
Right femoral head and partial neck	51
Right distal femur	63
Right patella (2 conjoined pieces)	79, 100
Right proximal tibia (2 conjoined pieces)	64, 78
Right distal tibia	97
Left proximal tibia fragment	24
Left proximal fibula (2 conjoined pieces)	23, 84
Left distal fibula[d]	76
Right talus	98
Right calcaneus	99
Pedal proximal phalanx[d]	91
Pedal distal phalanx	111

a. While all of the material recovered from Malapa is considered to represent *Au. sediba*, attribution of elements to specific individuals is subject to change.
b. Catalogue numbers assigned for individual sites based on the University of the Witwatersrand collections numbering system (*31*). Malapa is designated site UW88, therefore all numbers indicated above are preceded by the prefix UW88-.
c. Attribution to MH1 uncertain.
d. Attribution to MH2 uncertain.

Table S2: Phenetic comparisons of postcranial morphology in *Australopithecus* and early *Homo*. The postcranial features described in this table are not intended as an exhaustive list of the morphological attributes of the Malapa hominin postcranial skeletons. Postcranial character states for various taxa were derived from the literature where noted, otherwise data derive from measurements and observations by the authors on the original fossil material, or, in the case of specimens from Hadar and Olduvai Gorge, casts.

	Au. afarensis[a]	***Au. africanus***[b]	***Au. sediba***	***H. habilis***[c]	***H. sp. indet.***[d]	***H. erectus***[e]
BODY PROPORTIONS						
Body size (femoral head SI diameter)	Variable (but generally small) (28.6 – 39.4) (*32*)	Variable (but generally small) (30.8 – 38.4) (*33*, *34*)	Small (29.8[f] – 32.7)	Small? (*35*)	Large (38.9 – 42.6)	Variable (but generally large) (33.4 - 46.1) (*6*, *36-38*)
Brachial index	72.8-90.7(*39*)	-	84.3	79.5-93.2(*39*)	-	79.9(*37*)
Relative humeral length (humeral length/femoral head diameter)[g]	Long 9.23	-	Intermediate 8.15 – 8.23	-	-	Short 6.93 – 7.38
Humeral-to-femoral diaphyseal strength (humeral mid-proximal/femoral midshaft polar section modulus)	-	-	0.383[h]	0.590[i] (*40*)	-	0.303-0.442 (*41*)
Upper-to-lower limb joint size proportions (humeral distal articular breadth/femoral head diameter)	Large (1.05)	Large (1.11)[j]	Large (1.08)	-	-	Small (0.88)
CLAVICLE						
Angle of acromial extremity to plane of shaft	-	Anterosuperiorly inflected	Anterosuperiorly inflected	Uninflected	-	Anterosuperiorly inflected
Conoid tubercle	Angular margin(*42*)	Angular margin	Angular margin	Weak/absent tubercle	-	Weak/absent tubercle
Mid-lateral shaft cross-sectional shape	Dorsoventrally-elongated oval (*42*)	Dorsoventrally-elongated oval	Dorsoventrally-elongated oval	Rounded	-	Variably dorsoventrally-elongated oval or rounded

SCAPULA						
Spine thickness	Moderately thick(*43*)	Moderately thick	Moderately thick	Thick(*43, 44*)	-	Moderately thick(*43*)
Axillary border ventral pillar	Strongly developed	Strongly developed	Strongly developed	-	-	Moderately developed
Axilloglenoid angle	116°	115°(*36*)	114°	-	-	128°(*36*)
HUMERUS						
Midshaft (40-50%) xsect %CA	-	63-74	75[k]	79.7(*40*)	-	81.7(*40*)
Humeral torsion	124°	126°	103°	-	-	110° - 126°(*36*)
Projection of medial epicondyle (medial epicondyle /biepicondylar breadth)	Weak-moderate (0.16 – 0.25)	Moderate (0.25)	Strong (0.31)	Strong(*45*) (0.29)	-	Strong (0.32)[l]
Lateral epicondyle	Moderately projecting, proximally-positioned	Pronounced, proximally-positioned	Pronounced, proximally-positioned	Pronounced, proximally-positioned	-	Moderately projecting, distally-positioned
Brachioradialis crest	Variable	Marked	Marked	-	-	Weak
Septal aperture (supratrochlear foramen)	Present	Absent	Present	Present(*45*)	-	Absent
Supracapitular fossa	Moderate	Moderate	Moderate to deep	Well excavated(*45*)	-	Shallow
Olecranon fossa	Relatively large and deep	Relatively narrow and deep	Relatively large and deep	Relatively large and deep (contra (*46*))	-	Relatively narrow and shallow
Capitular morphology (Capitular superoinferior breadth/ humeral distal articular breadth)	Superoinferiorly elongated (0.42)	Superoinferiorly elongated (0.43)	Superoinferiorly elongated (0.43-0.44)	Superoinferiorly elongated (0.47)	-	Moderately superoinferiorly elongated (0.40)
Trochlear/capitular keel	Marked	Marked	Marked	Marked(*45*)	-	Moderate
RADIUS						
Head diameter/neck length	0.38	0.60	(0.50)	0.49	-	-

ULNA						
Orientation of trochlear notch	Anterior (*47*) to Anteroproximal	Anteroproximal	Anteroproximal	-	-	Anterior
M. flexor carpi ulnaris tubercle	Weak-moderate	Pronounced	Pronounced	-	-	Weak-moderate
Trochlear keel	Mild (*47*)	Mild	Mild	-	-	Moderate
Orientation of plane of radial notch	Slight proximolateral	Slight proximolateral	Slight proximolateral	-	-	Lateral
M. flexor digitorum superficialis origin	Crest	Crest	Crest	-	-	Tubercle
Supinator crest	Weak	Moderate	Moderate	-	-	Prominent
Mid-proximal diaphyseal shape	Rounded	Laterally-flattened triangle	Laterally-flattened "D"	-	-	Anteriorly-flattened triangle
Interosseous crest	Moderate	Weak	Weak	-	-	Prominent
OS COXA						
Acetabulocristal buttress	Slight-to-absent	Slight-to-absent	Pronounced[k]	-	Pronounced	Pronounced
Position of cristal tubercle	Anterior	Anterior	(Posterior)[k]	-	Posterior	Posterior
Iliac crest shape	Shallow sigmoid	Shallow sigmoid	(moderate sigmoid)[k]	-	Deep sigmoid	Deep sigmoid
Anterior inferior iliac spine shape	Rectilinear	Rectilinear	Sigmoid[k]	-	Sigmoid	Sigmoid
Posterior fossa for M. gluteus medius	Small	Moderately expanded	Moderately expanded[k]	-	Expanded	Expanded
Posterior iliac height	Short	Intermediate	Tall[k]	-	Tall	Tall
Retroauricular area	Short	Short	Expanded[k]	-	Expanded	Expanded
Tuberoacetabular sulcus	Wide	Wide	Narrow[k]	-	Narrow	Narrow
Relative tuberoacetabular sulcus width (TAS/acetabular width)[m]	0.50(*48*)	0.52	0.29	-	0.25	-
Relative auricular-acetabular distance (acetabuloauricular distance/femoral head SI diameter)[n]	Long (1.68)	Long (1.62)	Intermediate[k] (1.31)	-	Short (1.12-1.15)	Short (1.00)

Acetabulosacral buttress	Moderate	Small	Pronounced[k]	-	Pronounced	Pronounced
Minimum thickness of acetabulosacral buttress(*19*)	15.5	13.9	18.0	-	20-26(*49*)	19.2
Retroauricular height (posterior superior iliac spine to junction of the two limbs of the auricular area of posterior border)	(30)	33	≥ 50.5	-	52-53(*49*)	(47)
Pubic symphyseal face	Short, ovoid(*6*)	Short(*6*)	Tall, thin	-	Tall, thin(*6*)	Tall, thin(*6*)
FEMUR						
Relative neck length (neck length[o]/femoral head SI diameter)	1.14	0.951-1.442 (*34*)	1.02[k]		1.06-1.12	1.26[p]
Neck-shaft angle	Variably high (117°-125°)(*32*, *50*)	Variably high (118° - 122°)	Low[k] (115°)	High (123°)(*35*)	Moderate (118°-119°)	Low (110°-115°)
Neck shape index (100* neck AP/SI diameter)	68.7-86.9(*51*)	73.4(*51*)	69.4[k]	-	73.6-79.0	73.7
Neck cross-sectional long axis	Superoinferiorly oriented	Superoinferiorly oriented	Anterosuperior to posteroinferiorly oriented[k]	Superoinferiorly oriented	Moderately anterosuperior to posteroinferiorly oriented	Moderately anterosuperior to posteroinferiorly oriented
Proximal diaphyseal cross-sectional shape	Mediolaterally expanded but not buttressed	Strongly mediolaterally buttressed	Mediolaterally expanded but not buttressed[k]	Approx. circular(*10*)	Strongly mediolaterally buttressed	Strongly mediolaterally buttressed(*10*)
Meric index (proximal diaphyseal AP/ML diameter)	66.7 - 71.6(*35*, *50*)	74.1	79.6[k]	1.00(*35*)	71.0 - 74.3	74.1
Midshaft-to-mid-proximal (50-65%) xsect %CA	-	(80)	84.4[h]	83.2(*50*)	85.6(*52*)	65.2-86.8(*40*, *41*)
pilaster	Variably present(*32*, *53*)	Well-developed	Absent[k]	Well-developed(*40*, *43*, *54*)	Absent	Slight

Linea aspera	Weak(*32*, *53*)	Weak	Weak[k]	Prominent(*45*)	Prominent	Prominent
TIBIA						
Popliteal (soleal) line	Prominent(*32*)	Prominent(*55*)	Moderate?[k]	Strongly marked(*56*)	Marked?	Marked
Proximal shaft curvature	Slight, convex medially	Absent	Absent[k]	Slight, convex medially(*56*)	Absent	Absent
Diaphyseal anterior border	Rounded?	-	Sharp[k]	Rounded (*56*)	Sharp?	Rounded
Midshaft relative muscle attachment size (midshaft)	-	-	Flexor digitorum longus ≅ tibialis posterior[k]	Tibialis posterior > flexor digitorum longus(*56*)	-	Flexor digitorum longus > tibialis posterior
Distal shaft curvature	Slight (convex laterally) to absent	-	Slight, convex laterally[k]	Slight, convex laterally(*56*)	-	Slight, convex laterally
Morphology of triangular attachment area for inferior interosseous ligament	Poorly marked, superoinferiorly short	Poorly marked, superoinferiorly short	Poorly marked, superoinferiorly short	Well-marked and elongate(*56*)	Well-marked and elongate	Poorly marked, elongate
Distal tibiofibular articular facet	Small and cresentic	Small and cresentic	Small and cresentic	Small and cresentic(*56*)	L-shaped (superoinferiorly expanded anteriorly)	Superinferiorly narrow rectangle
Talar articular surface orientation (as seen in lateral view)	Variably anteriorly or posteriorly tilted(*18*)	Variably anteriorly tilted or neutral	Anteriorly tilted	Anteriorly tilted(*56*)	Neutral (90°)	Neutral (90°)
FIBULA						
Malleolar breadth	Broad	-	Broad	Narrow(*56*)	Broad	Narrow?[q]
Distal tibiofibular articular facet	Small and cresentic	-	Rectangular	Small and cresentic(*56*)	Oval	-
Talar articular surface orientation	Laterally sloping	-	Vertical	Vertical(*56*)	Vertical	-
FOOT[r]						
Talar trochlear surface	Flat (references in (*57*))	Flat to slightly grooved	Flat	Deeply grooved(*58*)	-	Deeply grooved

Talar trochlear medial and lateral radii of curvature	Roughly equal (references in (*57*))	Roughly equal to elevated medial margin	Roughly equal	Roughly equal(*59*)	-	Elevated lateral margin
Talar medial malleolar surface	Extends onto talar neck	Extends onto talar neck	Does not extend onto neck	Extends onto talar neck(*60*)	-	Does not extend onto neck
Talar neck	Short, stout, medially twisted	Short, stout, medially twisted	Short, stout, medially twisted	Short, stout, medially twisted(*60*)	-	Longer, less robust, not twisted
Talar head/neck orientation angle	Neutral (90°)	Neutral (90°)	Neutral (90°)	Valgus deviation (75°)(*60*)	-	Varus deviation (105°)
Horizontal angle of talar neck	21°	21°-26°	28°	28°(*60*)	-	15°-26°(*36*)
Angle of inclination of talar neck	10°	11°	30°	8° (*60*)	-	(16°)
Talar neck torsion angle	25°	21°	29°	40° (*60*)	-	40°
Talar fibular facet/neck length index	195	182	181	125(*60*)	-	132
Talar head projection index	37	(37)	61	45 (*60*)	-	-
Talar trochlear breadth/length index	87	80	72	100 (*60*)	-	(84)
Talar trochlear breadth/fibular facet projection index	253	336	267	330 (*60*)	-	239
Calcaneal fossa on inferomedial surface for cuboid projection	-	-	Absent	Present(*61*)	-	-
Metatarsal diaphyses	Gracile	Gracile	Gracile	Robust(*58*)	-	Gracile(*36*)

a. As represented by AL 137-48A, AL 211-1, AL 288-1, AL 322-1, AL 333-3, AL 333-4, AL 333-6, AL 333-7, AL 333-9a, AL 333-9b, AL 333-75, AL 333-85, AL 333-95, AL 333-111, AL 333w-37, AL 333X-6/9, AL 333x-26, AL 438-1, Mak VP 1/1 and Mak VP 1/3.
b. As represented by MLD 46, Sts 7, Sts 14, Stw 25, Stw 88, Stw 99, Stw 102, Stw 181, Stw 311, Stw 347, Stw 358, Stw 363, Stw 389, Stw 392, Stw 403, Stw 431, Stw 443, Stw 479, Stw 486, Stw 501, Stw514, Stw 522, Stw 527, Stw 573, and Stw 598.
c. *H. habilis* postcranial hypodigm taken as OH7, OH8, OH35, OH 48, OH62 and KNM ER 3735.
d. Postcranial material conventionally considered to represent early *Homo*, but without associated taxonomically-diagnostic craniodental remains: KNM ER 1472, KNM ER 1475, KNM ER 1481, KNM ER 3228 and OH 28.

e. *H. erectus (ergaster)* represented by KNM WT 15000, KNM ER 813, KNM ER 1808, KNM BK 66, BSN49/P27, and postcranial material from Dmanisi possibly associated with the D2600 cranium (D4166, D4161, D4507, D4167, D3901, D4110, D2021, D4165, D4058).

f. As determined from the epiphyseal plate. Observation of adult femora reveals that the points defining the maximum SI diameter of the head correspond, both superiorly and inferiorly, with the line of fusion of the head epiphysis. Therefore the measurement taken on the epiphyseal plate should correspond closely with the actual SI diameter of the head at the time of death. We note also that further appositional growth of the articular surface up until skeletal maturity may have increased this dimension somewhat.

g. We note that femoral head size tends to be smaller relative to body size in *Australopithecus* compared to *Homo*, which exaggerates somewhat the perception of long arms in *Australopithecus* in the ratio presented here. If the Malapa hominins share with *Australopithecus* the trait of small femoral heads relative to body mass, their relative humeral length would be slightly closer to that observed in *Homo* (thus they would be more *Homo*-like in relative upper limb length, but more *Australopithecus*-like in relative femoral head size).

h. Damage to the midshaft necessitated use of the mid-proximal diaphysis (at about 70% of biomechanical length, from the distal end) in MH1. Given uniformity in diaphyseal diameters and cortical thickness from this location down to the approximate midshaft, the use of this location is not expected to significantly bias the comparison with other taxa. It should also be noted that MH1 was a juvenile at the time of death (but comparable in age to KNM-WT 15000, whose values are also used), and that adult values may differ. We also note that lack of knowledge of femoral biomechanical length hinders the interpretation of relative upper-to-lower limb strength ratios. Rather than using dubious estimates of femoral length, we instead follow the logic outlined in (*40*) and limit this comparison to a ratio of unstandardized humeral to femoral dimensions.

i. Section locations taken between 40-50% of biomechanical length for the humerus, and 50-65% of biomechanical length for the femur (*40*).

j. No *A. africanus* specimen preserves both a distal humerus and a femoral head, although Stw 431 preserves a distal humerus and an acetabulum. Femoral head diameter for this specimen was estimated from the diameter of the acetabulum as 36 mm (*62*).

k. Based on morphology observable in MH1 juvenile. Additional growth and development to skeletal maturity would have potentially altered morphology.

l. Estimated from photograph in (*36*).

m. TAS = minimum width of the tuberoacetabular sulcus. Based on values provided by (*48*), the two Australopith specimens – AL 288-1 and Sts 14 - for which TAS and acetabular width (AD) can be measured have TAS/AD ratios that are 3.5 and 3.7 standard deviations, respectively, above the mean ratio in a sample of 98 modern humans. AL 288-1 and Sts 14 also fall 6.6 and 6.9 standard deviations, respectively, above the mean value obtained for a sample of 18 modern human females. The early *Homo* sample (KNM-ER 3228 and OH 28, both with ratios = 0.25) falls within one standard deviation of both the pooled sex and the female modern human samples. Acetabular diameter in MH1 was estimated from the fossil as between 33 and 35.5 mm: we have used the lower value to produce the most conservative (least *Homo*-like) value possible. The value obtained falls within one standard deviation of the pooled sex sample of modern humans, but 1.6 standard deviations above the modern human female mean.

n. Acetabuloauricular distance = instrumentally determined minimum distance from margin of auricular surface to the lunate surface. Femoral head SI dimensions were estimated for some specimens (Sts 14, OH 28, ER 3228) from acetabular maximum diameter. Os coxa measurements for some specimens (AL 288-1 and OH 28) were taken on casts.

o. Intertrochanteric crest to junction between head and neck (*63*).

p. The ratio provided is based on KNM WT 15000, which clearly has a long femoral neck relative to the size of the femoral head (and which would have likely gotten longer with continued growth to skeletal maturity). However, the illustration of the D4167 femur (*5*) suggest that this trait may have been variable in early *H. erectus.*

q. As judged from the distal fibular metaphysis of KNM WT 15000.

r. Dimensions of the talus were obtained from a 3D virtual reconstruction of the partial foot skeleton of MH2, as illustrated in SOM Figure S5.

REFERENCES

1. P.H.G.M. Dirks, J.M. Kibii, B. F. Kuhn, C. Steininger, S.E. Churchill, J.D. Kramers, R. Pickering, D.L. Farber, A.S. Mériaux, A.I.R. Herries, G.C. P. King, L.R. Berger, *Science* **XXX**, XXX (2009). Companion paper.

2. L. Scheuer, S. Black, *The Juvenile Skeleton* (Elsevier Academic Press, London, 2004).

3. R. L. Susman, *Am. J. Phys. Anthropol*. **137**, 356 (2008).

4. B. H. Smith, in *The Nariokotome Skeleton,* A. C. Walker, R. E. F. Leakey, Eds. (Harvard University Press, Cambridge, 1993), pp. 195-220.

5. P. L. Walker, *Am. J. Phys. Anthropol.* **127**, 385 (2005).

6. S. W. Simpson *et al.*, *Science* **322**, 1089 (2008).

7. D.C. Johanson et al., *Am. J. Phys. Anthropol*. **57** (1982) (all papers within).

8. B. Asfaw, T. White, O. Lovejoy, B. Latimer, S. Simpson, G. Suwa, *Science* **274**, 629-635 (1999).

9. P. V. Tobias, *The Cranium and Maxillary Dentition of* Australopithecus (Zinjanthropus) boisei (Cambridge University Press, Cambridge, 1967).

10. A.W. Keyser, *S. Afr. J. Sci*. **96**, 189-193 (2000).

11. A.W. Keyser, C.G. Menter, J. Moggi-Cecchi, T.R. Pickering, L.R. Berger, *S. Afr. J. Sci.* **96**, 193-197 (2000).

12. P. V. Tobias, *Olduvai Gorge Volume 4: the Skulls, Endocasts and Teeth of* Homo habilis (Cambridge University Press, Cambridge, 1991).

13. N. T. Boaz, F. C. Howell, *Am. J. Phys. Anthropol*. **46**, 93 (1977).

14. W. H. Kimbel, D. C. Johanson, Y. Rak, *Am. J. Phys. Anthropol*. **103**, 235 (1997).

15. R. J. Blumenschine et al., *Science* **299**, 1217 (2003).

16. T. G. Bromage, F. Schrenk, F. W. Zonneveld, *J. Hum. Evol.* **28**, 71 (1995).

17. R. J. Clarke, Unpublished PhD dissertation, University of the Witwatersrand, Johannesburg (1977).

18. R. J. Clarke, *S. Afr. J. Sci*. **104**, 443 (2008).

19. F. E. Grine, B. Demes, W. L. Jungers, T. M. Cole. *Am. J. Phys. Anthropol*. **92**, 411 (1993).

20. F. E. Grine, W. L. Jungers, J. Schultz, *J. Hum. Evol.* **30**, 189 (1996).

21. F. Weidenreich, *Palaeontologia Sinica* **10**, 1 (1943).

22. G. Suwa et al, *Nature* **389**, 489 (1997).

23. A. Rosas, J. M. Bermudez de Castro, *Am. J. Phys. Anthropol*. **107**, 145 (1998).

24. S. C. Anton, *Yrbk. Phys. Anthropol*. **46**, 126 (2003).

25. G. P. Rightmire, D. Lordkipadnize, A. Vekua, *J. Hum. Evol.* **50**, 115 (2006).

26. A. H. Weaver, *Proc. Nat. Acad. Sci.* **102** (10), 3576 (2002).

27. K. J. Carlson, *Am. J. Phys. Anthropol*. **127**, 312 (2005).

28. K. J. Carlson et al., *Int. J. Primatol*. **29**, 1401 (2008).

29. K. J. Carlson et al., in *Primate Locomotion: Linking Field and Laboratory Research*, E. Vereecke, K. D'Aout, Eds. (Springer Press, Berlin, in the press).

30. B. Wood, *Koobi Fora Research Project, Volume 4: Hominid Cranial Remains* (Clarendon Press, Oxford, 1991).

31. B. Zipfel, L. R. Berger, *Palaeont. Afr*. **44**, 77 (2009).

32. C. O. Lovejoy, D. C. Johanson, Y. Coppens, *Am J Phys Anthropol* **57**, 679 (1982).

33. H. M. McHenry, *Am J Phys Anthropol* **87**, 407 (1992).

34. E. Harmon, *J Hum Evol* **56**, 551 (2009).

35. D. C. Johanson *et al.*, *Nature* **327**, 205 (1987).

36. D. Lordkipadnize *et al.*, *Nature* **449**, 305 (2007).

37. A. C. Walker, R. E. Leakey, in *The Nariokotome Skeleton,* A. C. Walker, R. E. Leakey, Eds. (Harvard University Press, Cambridge, 1993), pp. 95-160.

38. F. Spoor *et al.*, *Nature* **448**, 688 (2007).

39. B. G. Richmond, L. C. Aiello, B. A. Wood, *J Hum Evol* **43**, 529 (2002).

40. C. Ruff, *Am J Phys Anthropol* **138**, 90 (2009).

41. C. Ruff, *J Hum Evol* **54**, 383 (2008).

42. C. O. Lovejoy, D. C. Johanson, Y. Coppens, *Am J Phys Anthropol* **57**, 637 (1982).

43. M. Haeusler, H. M. McHenry, *J Hum Evol* **53**, 383 (2007).

44. R. E. Leakey, A. Walker, C. V. Ward, H. M. Grausz, in *Hominidae: Proceedings of the 2nd International Congress of Human Paleontology,* G. Giacobini, Ed. (Jaca Book, Turin, 1989), pp. 167-173.

45. R. E. F. Leakey, A. C. Walker, *Am J Phys Anthropol* **67**, 135 (1985).

46. R. E. Leakey, A. Walker, in *Hominidae: Proceedings of the 2nd International Congress of Human Paleontology,* G. Giacobini, Ed. (Jaca Book, Turin, 1989), pp. 209-215.

47. M. S. M. Drapeau, C. V. Ward, W. H. Kimbel, D. C. Johanson, Y. Rak, *J Hum Evol* **48**, 593 (2005).
48. J. T. J. Stern, R. L. Susman, *Am J Phys Anthropol* **60**, 279 (1983).
49. M. D. Rose, *Am J Phys Anthropol* **63**, 371 (1984).
50. C. O. Lovejoy, R. S. Meindl, J. C. Ohman, K. G. Heiple, T. D. White, *Am J Phys Anthropol* **119**, 97 (2002).
51. K. E. Reed, J. W. Kitching, F. E. Grine, W. L. Jungers, L. Sokoloff, *Am J Phys Anthropol* **92**, 1 (1993).
52. F. E. Grine, W. L. Jungers, P. V. Tobias, O. M. Pearson, *Am. J. Phys. Anthrop.* **97**, 151 (1995).
53. D. C. Johanson *et al.*, *Am J Phys Anthropol* **57**, 403 (1982).
54. M. Haeusler, H. M. McHenry, *J Hum Evol* **46**, 433 (2004).
55. L. R. Berger, P. V. Tobias, *J Hum Evol* **30**, 343 (1996).
56. P. R. Davis, *Nature* **201**, 967 (1964).
57. J. T. J. Stern, R. L. Susman, *Am J Phys Anthropol* **60**, 279 (1983).
58. W. E. H. Harcourt-Smith, L. C. Aiello, *J Anat* **204**, 403 (2004).
59. M. H. Day, J. R. Napier, *Nature* **201**, 969 (1964).
60. L. S. B. Leakey, P. V. Tobias, J. R. Napier, in *Nature*. (1964), vol. 202, pp. 7-9.
61. M. H. Day, B. A. Wood, *Man* **3**, 440 (1968).
62. R. L. Susman, J. T. Stern, *Science* **217**, 931 (1982).
63. H. M. McHenry, L. R. Berger, *J Hum Evol* **35**, 1 (1998).
64. L. C. Aiello, M. C. Dean, *An introduction to human evolutionary anatomy*. (Academic Press, London, 1990).